Numerical simulation of ground source heat pump system considering unsaturated soil properties and groundwater flow

Chaofeng Li [a], Peter John Cleall [b,*], Jinfeng Mao [a,*], José Javier Muñoz-Criollo [b]

[a] PLA University of Science and Technology, Nanjing 210007, PR China

[b] Cardiff School of Engineering, Cardiff University, Cardiff CF24 3AA, Wales, UK

* Corresponding author.

E-mail address: cleall@cardiff.ac.uk (P. J. Cleall)

Keywords: Ground source heat pump, Borehole heat exchanger, Unsaturated soil, Groundwater flow

ABSTRACT

This paper analyzes the influence of unsaturated soil properties and groundwater flow on the performance of ground source heat pump (GSHP) systems. A mathematical model of GSHP systems, which considers the influence varying unsaturated soil thermal properties, groundwater table depth and saturated groundwater flow, is introduced and coupled to a heat pump model to consider dynamically-changing loads due to specific heat pump coefficient of performance (COP) characteristics. The model is validated against experiment results and an analytical model reported by others. Finally, numerical simulations are performed to investigate the effect of inclusion of a heat pump, moisture content variations, groundwater table fluctuations and groundwater flow rates on the performance of the GSHP system. Results show that neglecting variations in moisture

content in unsaturated soil could lead to underestimating the heat transfer capacity of the soil. A rising groundwater tables is beneficial to the operation of the GSHP system. The influence of groundwater table fluctuation should be considered, otherwise could result in a maximum error of 3.78% on the outlet fluid temperature. When calculating the influence of groundwater flow rates on the performance of the GSHP system, the effect of groundwater tables should also be considered.

1. Introduction

Ground source heat pump (GSHP) systems are a promising and highly efficient renewable energy technology for space heating and cooling in buildings. This is due to the ground being able to provide a lower temperature, relative to the building space, when cooling is required, and a higher temperature when heating is required. Interseasonal temperature fluctuations in the soil are also smaller than that in the ambient air temperature [1,2]. A typical GSHP system generally consists of a geothermal heat pump and a ground heat exchanger (GHE). Typical GHE configurations can be classified into either horizontal or vertical types. Compared to horizontal types, vertical types (also known as borehole heat exchangers) are widely used especially in crowded urban areas, because their efficiency is much higher whilst also occupying less land [3]. However, installation cost for borehole heat exchangers (BHEs) is typically much higher, with drilling often accounting for half of the GSHP system installation cost [4]. A further consideration is that the efficiency of the heat pump is strongly dependent on the correct sizing of BHEs. Thus, correct analysis of heat transfer in BHEs is important in achieving optimum performance with minimum costs [5].

Over the years, many analytical and numerical models have been developed to estimate the

heat transfer capacity of BHEs. Classic analytical solutions often used are the line and cylindrical source models [6,7]. Based on the cylindrical source model, Bernier et al. [8] presented a multiple load aggregation algorithm to calculate the yearly performance of a BHE system subjected to hourly load variations. Eskilson [9] proposed a finite line source model for a BHE with finite length by using the finite-difference method. Subsequently, Zeng et al. [10] improved this approach by imposing a constant temperature at the ground surface to the finite line source model. In recent years, with the development of computers and numerical methods, numerical simulation studies are widely used. These studies are mainly based on finite difference, finite volume and finite element methods [11-13].

Generally, all or part of a BHE is located above the groundwater table [14,15]. Also in some cases, groundwater flow may be present in the saturated regions, which has the potential to greatly influence the heat transfer behavior of BHEs [16,17]. However, most existing models either regard the heat transfer between BHEs and their surrounding ground as a pure heat conduction process or assume the ground to be a fully saturated homogeneous porous. Few reported models consider the effect of layered ground conditions on the heat transfer of BHEs, especially when BHEs are partially located below the groundwater table where groundwater seepage is occurring [18,19]. In such cases, the combined effect of unsaturated soil properties above the groundwater table and groundwater flow below should be considered. Furthermore, in practice the location of the groundwater table may vary, due to seasonal changes in infiltration, runoff, evapotranspiration, agricultural irrigation or other factors [20], which will affect the heat transfer behavior of BHEs. However, this issue has not been widely considered or quantified in the literature.

Studies have shown that the initial distribution of undisturbed ground temperature, axial heat

transfer and ground surface temperature fluctuations have a significant influence on the performance of BHEs [21], especially for short borehole depths and long-term operation [22]. Bidarmaghz et al. [23] developed a 3D numerical model to investigate the effects of ground surface air temperature variations on BHEs. They reported that considering surface air temperature fluctuations may result in designed BHEs being up to 11% shorter BHEs than when ignored. Rivera et al. [24] expanded an existing finite line source model by implementing a more general Cauchy-type top boundary condition to study the influence of heat fluxes at the ground surface. They found that the difference in the calculated borehole wall temperature due to this more correct consideration of different boundary conditions at the surface was generally greater than 5% for short BHEs (< 50 m) and so it is clear that considering these factors when calculating the heat transfer of BHEs will lead to more accurate analyses.

BHEs are almost always utilized as part of a GSHP system [25,26]. When the heat pump is added, the thermal load of the BHE is influenced by the heat pump coefficient of performance (COP) [27]. The COP depends on both the building heat/cold demand and the performance characteristics of a specific heat pump. When the heat pump operates for heating, the thermal load of the BHE is lower than that of the building, whilst in cooling mode the thermal load of the BHE is higher. Typically, the heat pump COP is not constant and depends on the condition of the heat pump, condensation temperature and evaporation temperature. This variation is usually represented by a function based on heat pump inlet fluid temperature [28].

This paper describes a mathematical model of GSHP systems, which considers the influence of depth varying unsaturated soil thermal properties, groundwater table depth and saturated groundwater movement. The initial geothermal gradient and axial heat transfer are also

considered. Furthermore, a heat pump model is included to consider dynamically-changing loads due to specific COP characteristics. The model is validated against experiment results and analytical model reported by others that considers multiple-layer substrates and groundwater flow. The validated model is then applied to perform numerical simulations to investigate the effect of inclusion of a heat pump, moisture content variations, groundwater table fluctuations and groundwater flow rates on the performance of the GSHP system.

2. Method

A general numerical model is presented which represents phenomena in occurring in a GSHP system. The model considers three main elements of behavior, namely: heat transfer within the BHE, heat transfer into and within the adjacent ground and the coupling of the BHE to a heat pump. Heat transfer related to the BHE is composed of heat convection between the circulating fluid and the pipe and heat conduction in the pipe wall. Heat transfer in the adjacent ground is described by a transient heat transfer model in porous media, with the thermal properties of the ground define by a three-phase soil model that considers variation of properties with depth. The coupling of the heat pump and BHE is achieved via consideration of inlet and outlet fluid temperatures and is described via definition of suitable boundary conditions. A diagram of a typical GSHP system under consideration is shown in Fig. 1.

2.1. Model equations

2.1.1. Heat transfer of the BHE

The energy equation for fluid flow in a pipe can be written as [29]:

$$\rho_f A_p c_{p,f} \frac{\partial T_f}{\partial t} + \rho_f A_p c_{p,f} u \cdot \nabla T_f = A_p k_f \nabla \cdot \left(\nabla T_f \right) + \frac{1}{2} f_D \frac{\rho_f A_p}{d_h} |u|^3 + Q_{\text{wall}} \qquad (1)$$

where ρ_f is the fluid density, A_p is the cross section area of pipe, $c_{p,f}$ is the fluid heat capacity, T_f is

the temperature of circulating fluid, t is the time, u is the circulating fluid velocity, k_f is the fluid thermal conductivity, f_D is the Darcy friction factor that can be obtained from the Moody chart, d_h is the hydraulic pipe diameter. Furthermore, Q_{wall} indicates the heat transfer between the pipe and the surrounding ground and can be expressed as:

$$Q_{\text{wall}} = h_{\text{eff}} \left(T_{\text{ext}} - T_f \right) \tag{2}$$

where h_{eff} is the equivalent convective heat transfer coefficient of the pipe wall, T_{ext} is the temperature outside the pipe. For a circular pipe, h_{eff} can be described as:

$$h_{\text{eff}} = \frac{2\pi}{\frac{1}{r_i h_i} + \frac{\ln\left(\frac{r_o}{r_i}\right)}{k_p}} \tag{3}$$

where r_i and r_o are internal and external radiuses of the pipe respectively, k_p is the pipe thermal conductivity, h_i is the convection coefficient inside the pipe that can be obtained from：

$$h_i = \text{Nu} \frac{k_f}{d_h} \tag{4}$$

where Nu represents the Nusselt number which has a value of 3.66 in laminar and transitional conditions (Re<3000), and in turbulent conditions (Re>=3000) can be calculated by the Gnielinski correlation [29]:

$$\text{Nu}_{\text{turb}} = \frac{\left(f_D/8 \right)\left(\text{Re} - 1000 \right)\text{Pr}}{1 + 12.7\left(f_D/8 \right)^{1/2}\left(\text{Pr}^{2/3} - 1 \right)} \tag{5}$$

where Re is the Reynolds number, and Pr is the Prandtl number.

2.1.2. Heat transfer with the adjacent ground

When circulating fluid flows through the BHE, heat energy will firstly transfer to the grout and then the surrounding ground. As the volume of grout is relatively small compared to the ground and grout thermal properties are close to those of the ground, the approach of Yoon et al [30],

where the properties of the grout are taken to be the same as the surrounding ground, is adopted here.

The ground surrounding the BHE is regarded as a porous medium that can be defined as consisting of three phases, namely: solid, water and air. For the ground above the groundwater table, it is partially saturated, whilst the soil below the groundwater table can be regarded as being fully saturated. When the ground is fully saturated, the effect of the groundwater flow is considered in the heat transfer model. Transient heat transfer in porous media can be expressed as follows:

$$\left(\rho c_p\right)_{\text{eff}} \frac{\partial T}{\partial t} + \rho_w c_{p,w} v_w \cdot \nabla T = k_{\text{eff}} \nabla \cdot \left(\nabla T\right) - Q_{\text{wall}} \tag{6}$$

where T is the ground temperature, ρ_w is the density of groundwater, $c_{p,w}$ is the groundwater heat capacity, v_w is the groundwater flow velocity in saturated domain, and it is set as zero in unsaturated zone. $(\rho c_p)_{\text{eff}}$ and k_{eff} are effective volumetric heat capacity and effective thermal conductivity of the ground.

The thermal properties of ground can be affected by the inherent mineralogy and relative proportions of the three soil phases. Studies show that the variation of soil moisture content is a major factor that influences thermal conductivity of soil [31-33] and its distribution in unsaturated soil can be associated with soil suction via the soil water characteristic curve (SWCC). Soil suction is generally approximated by the matric suction [34] and ignoring moisture transfer in the unsaturated soil and assuming a hydrostatic pressure distribution, the matric suction profile above the groundwater table can be expressed as [35,36]

$$\psi = \left(u_a - u_w\right) = \rho_w g h \tag{7}$$

where ψ is the matric suction, u_a is the pore air pressure, u_w is the pore water pressure, g is the

acceleration due to gravity, and h is the height above the groundwater table.

The volumetric water content can be expressed by the Van Genuchten (VG) model as a function of matrix suction in the following form [37]:

$$\theta=\theta_r+\left(\theta_s-\theta_r\right)\left[\frac{1}{1+\left(a\psi\right)^n}\right]^m \tag{8}$$

where θ is the volumetric water content, θ_r is the residual water content, θ_s is the saturated water content, and a, n, and m are empirical fitting parameters that are related to air entry value, slope of curve, and shape of curve respectively. A common simplification is to assume m=1-1/n [38]. Thus the parameters in the model are θ_r ,θ_s , a, and n.

The volume fraction of each phase can be expressed as follows:

$$\chi_{\text{solid}}=1-\eta \tag{9}$$

$$\chi_{\text{water}}=\theta \tag{10}$$

$$\chi_{\text{air}}=\eta\text{-}\theta \tag{11}$$

where η denotes the soil porosity.

Effective thermal conductivity (k_{eff}) and effective volumetric thermal capacity ($(\rho c_p)_{\text{eff}}$) of the ground can be represented by either adding the corresponding thermal properties of the different constituents according to their volume fraction [39] or empirical equations between soil thermal properties and water content [40]. In this paper they are expressed as the sum of thermal conductivity and heat capacity of each phase according to their volume fractions [41]:

$$k_{\text{eff}}=\sum_{i=1}^{3}\chi_i k_i \tag{12}$$

$$\left(\rho c_p\right)_{\text{eff}}=\sum_{i=1}^{3}\chi_i\rho_i c_i \tag{13}$$

2.2. Initial and boundary conditions

2.2.1. Initial conditions

Initial conditions of the ground and circulating fluid are regarded being in equilibrium:

$$T\left(x,y,z,t\right)\big|_{t=0} = T_f\left(x,y,z,t\right)\big|_{t=0} \tag{14}$$

and are taken as being defined by the following relationship for the background soil temperature profile $T(z,t)$ at time t=0 [42]:

$$T\left(z,t\right) = T_{\text{mean}} - T_{\text{amp}} \exp\left(z\sqrt{\frac{\pi}{t_0 \alpha_{\text{eff}}}}\right)\cos\left(\frac{2\pi t}{t_0} - \varphi + z\sqrt{\frac{\pi}{t_0 \alpha_{\text{eff}}}}\right) \tag{15}$$

where T_{mean} is the annual average temperature, T_{amp} is the amplitude of annual temperature, t_0 is the period of one year, α_{eff} is effective ground thermal diffusivity, φ is phase angle.

2.2.2. Boundary conditions

Following the approach of [43] the upper (ground surface), bottom, and far field boundaries of the domain are fixed at the background soil temperature profile as defined by Eq. (15) and it should be noted that the computational soil domain should be large enough that the heat released by the BHE has negligible effect on the far-field boundary temperature.

$$T\left(x,y,z,t\right) = T\left(z,t\right) \tag{16}$$

The coupling of the heat pump and the BHE is achieved through consideration of inlet and outlet fluid temperatures. The inlet fluid temperature of the BHE can be computed using the outlet fluid temperature from the preceding time step by [44]:

$$T_{f,i} = T_{f,o} + \frac{Q_{\text{BHE}}}{\rho_f c_{p,f} V_f} \tag{17}$$

where $T_{f,i}$ and $T_{f,o}$ are inlet and outlet fluid temperatures, Q_{BHE} is the thermal load of the BHE, V_f is the volumetric flow rate.

In heating mode, the thermal load of BHE (Q_{BHE}) is lower than that of the building and it can be

expressed as:

$$Q_{\mathrm{BHE}}^{\mathrm{heating}} = Q_{\mathrm{Building}}\left(1-\frac{1}{\mathrm{COP}_{\mathrm{heating}}}\right) \tag{18}$$

and in cooling mode it can be expressed as:

$$Q_{\mathrm{BHE}}^{\mathrm{cooling}} = Q_{\mathrm{Building}}\left(1+\frac{1}{\mathrm{COP}_{\mathrm{cooling}}}\right) \tag{19}$$

Normally, the COP of a specific heat pump is not constant and is often represented as function of the heat pump inlet fluid temperature. In this work the relationship between the outlet fluid temperature of BHE and COP is assumed to be as defined by [45]:

$$\mathrm{COP} = a'T_{f,o}^2 + b'T_{f,o} + c' \tag{20}$$

2.3. Numerical solution

The numerical model is developed using an existing software platform [46] utilizing the finite element method for spatial discretization and a backward difference time stepping scheme. The coupling of each part of the proposed model and the calculation process are shown in Fig. 2.

3. Model verification and validation

The proposed numerical model is verified and validated against the experiment results and the analytical model proposed by Hu [47], in which the multiple-layer substrates and groundwater flow are considered. The experiment conducted by Hu was located in an area with a relatively complex geological structure, consisting of three layers from the top to the bottom, namely, backfill soil, clay and fine sand. The thickness of the three layers are 20, 18 and 25 m respectively, the groundwater table was at the ground surface. As reported in [47] there was no obvious groundwater flow in experiment area according to the geological report, the groundwater flow velocity was taken as 0 $m \cdot s^{-1}$. The borehole radius is 0.14 m. A U-shape BHE is installed inside the

borehole and its length, internal pipe radius, external pipe radius and pipe shank spacing are 63, 0.013, 0.016 and 0.06 m respectively. Details of the parameters of test site are shown in Table 1. As the analytical model used in the literature neglected the thermal capacity of the grout, it is assumed that the thermal capacity of the grout is equal to the arithmetic mean of the surrounding soil (2.71 $MJ{\cdot}m^{-3}{\cdot}°C^{-1}$) and thermal conductivity of the grout is 1.5 $W{\cdot}m^{-1}{\cdot}°C^{-1}$. Following the approach of Hu heat transfer in the grout is regarded as being purely conductive.

Fig. 3(a) shows the outlet fluid temperature calculated by proposed numerical model and the result reported by Hu [47]. Compared to the experiment result, the greatest relative error occurs at the beginning of the simulation, with the differences becoming smaller with time. Compared to the result calculated by Hu's model, the result calculated by present model is slight lower especially at the beginning the simulation. The reason for this phenomenon could be due to the consideration of the thermal capacity of the grout. As reported in the literature, the maximum error was less than 0.3 ℃ between Hu's model and the experiment result except for that of the first eight hours. The maximum error between proposed model and the experiment result is also less than 0.3 ℃.

The proposed model is further verified against Hu's analytical model when groundwater flow is considered. A groundwater flow rate of 6e-7 $m{\cdot}s^{-1}$ is assumed in lower two soil layers and no groundwater flow is assumed the upper backfill soil layer. The inlet fluid temperature is held constant at 30 ℃ and all other parameters used are as used in the previous analysis. Fig. 3(b) shows that the proposed model is in good agreement with results from Hu's analytical model, with the largest variation between the two results being below 0.1 ℃. From Section 2 it can also be seen that the proposed model has the benefit over alternative analytical solutions to be able

to consider a much wider range of problems, which are not constrained by limiting assumptions that are necessary to allow the analytical solution to be developed.

4. Investigation of system performance under some influence factors

In this section, numerical simulations are performed to investigate the effects of i) heat pump inclusion, ii) variations on moisture content, iii) groundwater table fluctuation and iv) groundwater flow in saturated soil on the performance of the GSHP system. As shown in Fig. 4, the computational soil domain is 20, 20, and 61 m in the x, y, and z (depth) directions respectively. The top of the U-shape BHE is 1 m beneath the ground surface and its length, internal pipe radius, external pipe radius and pipe shank spacing are 50, 0.014, 0.016 and 0.06 m respectively. As the pipeline exhibited a steep temperature gradient a relatively fine mesh was used near the pipe with a total of 44021 4-noded tetrahedral elements used. Spatial and temporal convergence of the solution was checked via trial and error with a time step of 1 hour found to be suitable. The ground is assumed to consist of a thick strata of silty loam and model parameters for the SWCC are taken from the UNSODA database [48]. Initial ground temperature profile and far-field boundary temperatures are represented by Eq. (14) and (16). The circulating fluid is water and parameters used in the numerical analysis are shown in Table 2. The resulting relationships defining the variation of thermal conductivity and heat capacity with volumetric water content are illustrated in Fig. 5.

The building load for the 50-m BHE is represented in a simplified way by a regular sinusoidal load with a period of one year, with unbalanced winter and summer loads, which following the approach of [49], can be expressed as:

$$Q_{\text{Building}} = \frac{3}{4}A_0 \sin\left(\frac{2\pi}{t_0}t\text{-}\varphi'\right) + \frac{1}{4}A_0\left|\sin\left(\frac{2\pi}{t_0}t\text{-}\varphi'\right)\right| \quad (21)$$

where A_0 is the highest magnitude of the load in each year and is taken as 3000 W, φ' is phase angle to control the beginning time of the system operation and is taken as zero here. The building load (Eq. (21)) and ground surface temperature ($T(0,t)$) are shown in Fig. 6 with a positive load value representing a cooling load. It should be noted that the peak cooling load and peak surface temperature occur at month 3 (as shown in Fig. 6), whilst peak heating load and lowest surface temperature occurs at 9 months.

In order to ensure convergence a mesh independence study was undertaken, Fig. 7 presents the highest outlet fluid temperatures from four different meshes with increasing element densities (with 30576, 36722, 40021 and 44021 elements respectively). The highest outlet temperature is used for comparison as this occurs when the building load is at its greatest and the outlet temperatures and the difference between them (for the 4 meshes considered) are also greatest. According to the test results, the highest outlet temperature tends to converge toward a constant value when the number of mesh elements exceeds 44021. The outlet temperature difference between the last two cases is about 0.01 ℃. Therefore, the mesh with 44012 elements was selected in this study.

4.1 Comparison between results with and without the heat pump

When a heat pump is included in the GSHP system, the load for the BHE will not be equal to the building load. In order to investigate the effect of inclusion of a heat pump on the performance of GSHP system, inlet and outlet fluid temperatures of the two cases (one with and another without the heat pump) are compared. In this analysis it is assumed that the groundwater table is at the mid height of the BHE, that is, the bottom half of the BHE is below the groundwater table, and that the groundwater flow rate is zero.

Comparison results are shown in Fig. 8. It can be seen that inlet and outlet fluid temperatures

are higher when the heat pump is considered no matter under cooling load or heating load. This is because the electricity consumed by the heat pump results in a temperature rise in the circulating water, which is detrimental to cooling but conductive to heating. To be more specific, the highest and lowest outlet fluid temperatures with and without considering the effect of heat pump are 33.55, 13.73 and 30.90, 12.36 ℃ respectively in a year. Without considering the effect of heat pump could underestimate the highest and lowest outlet temperature by 2.65 and 1.37 ℃. Thus, ignoring the effect of heat pump could result in the designed total length of the BHE being either shorter or longer than the requirements of the building if based on the cooling or heating load.

4.2 Effect of moisture in unsaturated soil

Moisture is a major factor influencing the soil thermal conductivity. When the soil porosity is constant, neglecting variations in moisture content distribution will underestimate the soil thermal conductivity, which could result in error when calculating the heat transfer of the BHE. Fig. 9 shows the outlet fluid temperatures and the corresponding heat pump COP when three cases for the distribution of moisture content are considered (groundwater table is defined as being at the mid height of the BHE for all cases): i) fully dry above the groundwater table (GWT), ii) varying moisture content (Eq. (8)) above the groundwater table and iii) fully saturated above the groundwater table (equivalent to the groundwater table at the ground surface). In order to study the effect of moisture on short BHEs, the performance of a 25-m BHE is also studied with a building load for the 25-m BHE being half that considered for the 50-m BHE. The depth of the 25-m BHE computational domain is 36 m (the number of 4-noded tetrahedral elements in the mesh is reduced to 25980 accordingly). It can be seen that for the 50-m BHE, the highest outlet fluid temperatures are 34.16,

33.56, 31.74 ℃ and the corresponding lowest heat pump COP are 4.196, 4.284 and 4.539 respectively in the three cases. Thus, neglecting the moisture in unsaturated soil could lead to overestimating outlet fluid temperatures in cooling season and making the designed BHE length longer than needed, therefore increasing initial investment. A similar conclusion can be found through analyzing the lowest outlet fluid temperatures.

From Fig. 9, it can also be seen that the highest outlet temperatures are 37.60, 36.74 and 34.63 ℃ for the 25-m BHE in the three cases. These results are higher than the corresponding ones for the 50-m BHE. Although heat fluxes per unit length are same for them. This could be due to shallow soil is susceptible to the ground surface temperature, the heat transfer rate for short BHEs is poorer than that for longer BHEs. Furthermore, it can also be concluded that the effect of ground surface temperature and moisture change on short BHEs is greater than long BHEs.

4.3 Performance at different levels of groundwater table

The effect of the groundwater table on the performance of GSHP system is investigated with Fig. 10 comparing outlet fluid temperatures and heat pump COP under three different positions of the groundwater table: i) groundwater table (GWT) below the BHE, ii) groundwater table at mid height of the BHE (Case ii in Section 4.2) and iii) groundwater table at the ground surface (Case iii in Section 4.2). Groundwater flow velocity is set as zero. The varying moisture content (Eq. (8)) above the groundwater table is considered in the first two cases in this section.

Taking the fluid temperature in cooling mode as an example, it can be seen that higher groundwater table leads to lower outlet temperature and higher heat pump COP. That is, the rise of groundwater table is beneficial to the operation of GSHP system. This is because the rising groundwater table results in the increase of soil thermal conductivity. When in heating mode,

higher groundwater table can also result in higher heat pump COP. Although, at the very beginning of the heating mode, the heat pump COP is the highest when the groundwater table is below the BHE.

4.4 Influence of groundwater table fluctuation

From above analysis, it can be seen that groundwater table could have much influence on the performance of GSHP system. However, groundwater table is not constant in a year in real cases. It may vary due to seasonal changes such as precipitation and evapotranspiration. Agricultural irrigation can also have an impact on the groundwater table. In order to study the impact of time-varying groundwater table on the performance of GSHP system, similarly to the building load (Eq. (21)), the groundwater table is simplified to a cosinusoidal shape curve [20]:

$$H_{GT} = A_1 + B_1 \cos\left(\frac{2\pi}{t_0} t + \varphi''\right) \tag{22}$$

where A_1 is the annual average groundwater table, B_1 is the amplitude of groundwater table, φ'' is phase angle.

Fig. 11 shows four kinds of groundwater table fluctuation curves in different places. i) groundwater table (GWT) is constant and is at mid height of the BHE (Case ii in Sections 4.2 and 4.3). Case ii, Case iii and Case iv are groundwater tables changing with time. The annual average groundwater tables are -26 m (equal to Case i), and the amplitudes are 20 m in the three cases. Case ii represents a lower groundwater table during the cooling season and a higher groundwater table during the heating season due to the evaporation and agricultural irrigation. Case iii represents that the highest and lowest groundwater tables occur in transition seasons due to seasonal rainfall. Case iv is the opposite of Case ii for snow melt.

Fig. 12 shows the outlet fluid temperatures and heat pump COP of four cases under unbalanced

load (Eq. (21)). It can be seen that although the average groundwater tables are same in four cases, there are big differences in the outlet temperatures and heat pump COP. For example, the highest outlet temperatures of four cases are 33.56, 34.33, 33.20, 32.29 ℃ and the corresponding lowest heat pump COP are 4.2845, 4.1708, 4.3365 and 4.4643 respectively. The outlet temperature of Case ii is 2.29 % higher than Case i, and Case iv is 3.78 % lower than Case i. The reason for it is that the varying groundwater table makes the ground thermal properties changing with time. Without considering the groundwater table fluctuation, the outlet temperature could be underestimated or overestimated. Therefore, when designing the BHE, the impact of groundwater table fluctuation should also be considered.

4.5 Effect of groundwater flow rates considering groundwater tables

Groundwater flow has a big influence on the heat transfer of BHEs. However, existing studies seldom consider the influence of groundwater table when studying the effects of groundwater flow. Fig. 13 shows the outlet fluid temperatures and heat pump COP under different groundwater flow rates. The effect of groundwater tables is also considered in two cases: groundwater table (GWT) at mid height of the BHE and groundwater table at ground surface.

Taking the groundwater table at mid height of the BHE as an example (black, red and blue lines), it can be seen that outlet fluid temperatures decrease and heat pump COP increases with the increase of groundwater flow rate in cooling mode (1 month to 6 month). However, at the beginning of the following heating mode (6 month to around 9 month) (enlarged part in the figure), it can be seen that higher groundwater flow rate leads to a lower outlet temperature, and lower heat pump COP. Thenceforth, the outlet fluid temperature and heat pump COP rise quickly with high groundwater flow rate (1e-6 $m \cdot s^{-1}$) overpassing those with low groundwater flow rates (1e-7

and 5e-7 m·s^{-1}). The reason for this phenomenon is that higher groundwater flow rates spreads the released heat downstream and the ground temperature tends to recover to its initial condition, which does not favor the operation of GSHP systems at the beginning of the opposite mode.

It can also be seen that when groundwater flow rates are 1e-7 and 5e-7 m·s^{-1}, the highest outlet fluid temperatures for the two groundwater tables are 33.53, 32.75 and 31.70, 30.40 ℃ respectively. Higher groundwater table leads to a lower outlet temperature, and a better performance. Analyzing the lowest outlet fluid temperature, we can get the same conclusion. Thus, when calculating the influence of groundwater flow on the performance of GSHP system, the influence of groundwater tables should also be considered.

5. Conclusion

In this paper, a general numerical model of GSHP system is introduced. The model considers relevant factors that influence the operation characteristics of GSHP systems. The model is validated against experiment results and analytical model in literature. Numerical simulations are carried out to investigate some factors that influence the operation of the GSHP systems. Main conclusions are as follows:

(1) As noted by others the effect of heat pump COP should be considered when analyzing the operation of the GSHP systems. If it is not considered the calculated inlet and outlet fluid temperatures will be underestimated and result in the designed total length of the BHE being either shorter or longer than necessary for the requirements of the building.

(2) Neglecting the moisture content in unsaturated region of the soil could lead to an underestimation of the heat transfer capacity of the soil and making the designed BHE length longer than needed. The effect of ground surface temperature and moisture change on short

BHEs is greater than long BHEs

(3) The rising of groundwater table is beneficial to the heat transfer of the BHE and the operation of the GSHP system.

(4) The influence of groundwater table fluctuation on the performance of BHEs should be noticed. The varying groundwater table makes the ground thermal properties changing with time, which could result in underestimate or overestimate of the outlet fluid temperature.

(5) When calculating the influence of groundwater flow rates on the performance of GSHP system, the influence of groundwater tables should also be considered.

Acknowledgement

This work was supported by PLA University of Science and Technology, Cardiff University and China Scholarship Council.

References

[1] H. Yang, P. Cui, Z. Fang, Vertical-borehole ground-coupled heat pumps: A review of models and systems, Applied Energy 87 (1) (2010) 16-27.

[2] Y. Noorollahi, R. Saeidi, M. Mohammadi, M. Hosseinzadeh, A. Amiri, The effects of Ground Heat Exchanger Parameters Changes on Geothermal Heat Pump Performance-A Review. Applied Thermal Engineering (2017).

[3] G. Florides, E. Theofanous, I. Iosif-Stylianou, S. Tassou, Modeling and assessment of the efficiency of horizontal and vertical ground heat exchangers, Energy 58 (2013) 655-663.

[4] C. Han, X. B. Yu, Sensitivity analysis of a vertical geothermal heat pump system, Applied Energy 170 (2016) 148-160.

[5] J. Luo, J. Rohn, M. Bayer, A. Priess, W. Xiang, Analysis on performance of borehole heat exchanger in a layered subsurface, Applied Energy 123 (2014) 55-65.

[6] L. R. Ingersoll, H. J. Plass, Theory of the ground pipe heat source for the heat pump, ASHVE transactions 47 (7) (1948) 339-348.

[7] H. S. Carslaw, J. C. Jaeger, Conduction of heat in solids, Oxford: Clarendon Press, 1959, 2nd ed. (1959).

[8] M. A. Bernier, P. Pinel, R. Labib, R. Paillot, A multiple load aggregation algorithm for annual hourly simulations of GCHP systems, Hvac&R Research 10 (4) (2004) 471-487.

[9] P. Eskilson, Thermal analysis of heat extraction boreholes, (1987).

[10] H. Y. Zeng, N. R. Diao, Z. H. Fang, A finite line - source model for boreholes in geothermal heat exchangers, Heat Transfer—Asian Research 31 (7) (2002) 558-567.

[11] E. Zanchini, S. Lazzari, New g-functions for the hourly simulation of double U-tube borehole heat exchanger fields, Energy 70 (2014) 444-455.

[12] S. Erol, M. A. Hashemi, B. François, Analytical solution of discontinuous heat extraction for sustainability and recovery aspects of borehole heat exchangers, International journal of thermal sciences 88 (2015) 47-58.

[13] D. Mottaghy, L. Dijkshoorn, Implementing an effective finite difference formulation for borehole heat exchangers into a heat and mass transport code, Renewable energy 45 (2012) 59-71.

[14] Z. Wang, F. Wang, Z. Ma, X. Wang, X. Wu, Research of heat and moisture transfer influence on the characteristics of the ground heat pump exchangers in unsaturated soil, Energy and Buildings 130 (2016) 140-149.

[15] G. A. Akrouch, M. Sánchez, J. L. Briaud, An experimental, analytical and numerical study on the thermal efficiency of energy piles in unsaturated soils, Computers and Geotechnics 71 (2016) 207-220.

[16] S. Geng, Y. Li, X. Han, H. Lian, H. Zhang, Evaluation of Thermal Anomalies in Multi-Boreholes Field Considering the Effects of Groundwater Flow, Sustainability 8 (6) (2016) 577.

[17] M. Mohamed, O. El Kezza, M. Abdel-Aal, A. Schellart, S. Tait, Effects of coolant flow rate, groundwater table fluctuations and infiltration of rainwater on the efficiency of heat recovery from near surface soil layers, Geothermics 53 (2015) 171-182.

[18] G. H. Go, S. R. Lee, N. V. Nikhil, S. Yoon, A new performance evaluation algorithm for horizontal GCHPs (ground coupled heat pump systems) that considers rainfall infiltration, Energy 83 (2015) 766-777.

[19] C. K. Lee, H. N. Lam, A modified multi-ground-layer model for borehole ground heat exchangers with an inhomogeneous groundwater flow, Energy 47 (1) (2012) 378-387.

[20] H. Ramesh, A. Mahesha, Simulation of Varada aquifer system for sustainable groundwater development, Journal of irrigation and drainage engineering 134 (3) (2008) 387-399.

[21] A. Zarrella, P. Pasquier, Effect of axial heat transfer and atmospheric conditions on the energy performance of GSHP systems: A simulation-based analysis, Applied Thermal Engineering 78 (2015) 591-604.

[22] M. S. Saadi, R. Gomri, Investigation of dynamic heat transfer process through coaxial heat exchangers in the ground, International Journal of Hydrogen Energy (2017).

[23] A. Bidarmaghz, G. A. Narsilio, I. W. Johnston, S. Colls, The importance of surface air temperature fluctuations on long-term performance of vertical ground heat exchangers, Geomechanics for Energy and the Environment 6 (2016): 35-44.

[24] J. A. Rivera, P. Blum, P. Bayer, A finite line source model with Cauchy-type top boundary conditions for simulating near surface effects on borehole heat exchangers, Energy 98 (2016) 50-63.

[25] S. Koohi-Fayegh, M. A. Rosen, An analytical approach to evaluating the effect of thermal interaction of geothermal heat exchangers on ground heat pump efficiency, Energy Conversion and Management 78 (2014) 184-192.

[26] C. Li, J. Mao, H. Zhang, Z. Xing, Y. Li, J. Zhou, Numerical simulation of horizontal spiral-coil ground source heat pump system: Sensitivity analysis and operation characteristics, Applied Thermal Engineering 110 (2017) 424-435.

[27] P. Hein, O. Kolditz, U. J. Görke, A. Bucher, H. Shao, A numerical study on the sustainability and efficiency of borehole heat exchanger coupled ground source heat pump systems, Applied Thermal Engineering 100 (2016) 421-433.

[28] H. Qian, Y. Wang, Modeling the interactions between the performance of ground source heat pumps and soil temperature variations, Energy for Sustainable Development 23 (2014) 115-121.

[29] T.L. Bergman, F.P. Incropera, A.S. Lavine, Fundamentals of Heat and Mass Transfer, John Wiley & Sons, 2011.

[30] S. Yoon, S. R. Lee, M. J. Kim, W. J. Kim, G. Y. Kim, K. Kim, Evaluation of stainless steel pipe performance as a ground heat exchanger in ground-source heat-pump system, Energy 113 (2016) 328-337.

[31] D. Kim, G. Kim, H. Baek, Thermal conductivities under unsaturated condition and mechanical properties of cement-based grout for vertical ground-heat exchangers in Korea—A case study, Energy and Buildings 122 (2016) 34-41.

[32] A. Moradi, K. M. Smits, J. Massey, A. Cihan, J. McCartney, Impact of coupled heat transfer and water flow on soil borehole thermal energy storage (SBTES) systems: Experimental and modeling investigation, Geothermics 57 (2015) 56-72.

[33] A. B. Platts, D. A. Cameron, J. Ward, Improving the performance of Ground Coupled Heat Exchangers in unsaturated soils, Energy and Buildings 104 (2015) 323-335.

[34] D. G. Fredlund, H. Rahardjo, Soil mechanics for unsaturated soils. John Wiley & Sons, 1993.

[35] J. C. Choi, S. R. Lee, D. S. Lee, Numerical simulation of vertical ground heat exchangers: intermittent operation in unsaturated soil conditions, Computers and Geotechnics 38(8) (2011) 949-958.

[36] N. Lu, W. J. Likos, Unsaturated soil mechanics. Wiley, 2004.

[37] M. T. Van Genuchten, A closed-form equation for predicting the hydraulic conductivity of unsaturated soils, Soil science society of America journal 44(5) (1980) 892-898.

[38] B. Ghanbarian-Alavijeh, A. Liaghat, G. H. Huang, M. T. Van Genuchten, Estimation of the van Genuchten soil water retention properties from soil textural data, Pedosphere 20(4) (2010) 456-465.

[39] S. W. Rees, M. H. Adjali, Z. Zhou, M. Davies, H. R. Thomas, Ground heat transfer effects on the thermal performance of earth-contact structures, Renewable and Sustainable Energy Reviews 4.3 (2000): 213-265.

[40] S. Lu, T. Ren, Y. Gong, R. Horton, An improved model for predicting soil thermal conductivity from water content at room temperature, Soil Science Society of America Journal 71.1 (2007): 8-14.

[41] S. E. Dehkordi, R. A. Schincariol, Effect of thermal-hydrogeological and borehole heat exchanger properties on performance and impact of vertical closed-loop geothermal heat pump systems, Hydrogeology Journal 22(1) (2014) 189-203.

[42] V. C. Mei, Heat transfer of buried pipe for heat pump application, Journal of solar energy engineering 113(1) (1991) 51-55.

[43] R. R. Dasare, S. K. Saha, Numerical study of horizontal ground heat exchanger for high energy demand applications, Applied Thermal Engineering 85 (2015) 252-263.

[44] L. Pu, D. Qi, K. Li, H. Tan, & Y. Li, Simulation study on the thermal performance of vertical U-tube heat exchangers for ground source heat pump system. Applied Thermal Engineering, 79 (2015) 202-213.

[45] I. Staffell, D. Brett, N. Brandon, A. Hawkes, A review of domestic heat pumps, Energy & Environmental Science 5(11) (2012) 9291-9306.

[46] COMSOL Multiphysics [Computer software]. COMSOL Inc., Burlington, MA.

[47] J. Hu, An improved analytical model for vertical borehole ground heat exchanger with multiple-layer substrates and groundwater flow, Applied Energy 202 (2017): 537-549.

[48] F. J. Leij, W. J. Alves, M. T. van Genuchten, J. R. Williams, The UNSODA unsaturated hydraulic database, US Environmental Protection Agency, Cincinnati, Ohio (1996).

[49] E. Zanchini, S. Lazzari, A. Priarone, Long-term performance of large borehole heat exchanger fields with unbalanced seasonal loads and groundwater flow, Energy 38 (2012) 66-77.

Nomenclature

A_0	highest magnitude of load (W)
A_1	annual average groundwater table (m)
A_p	cross section area of pipe (m^2)
a	fitting parameter of matrix suction function
a'	coefficient of COP function
B_1	amplitude of groundwater table (m)
b'	coefficient of COP function
c'	coefficient of COP function
$c_{p,f}$	circulating fluid heat capacity ($J \cdot kg^{-1} \cdot °C^{-1}$)
$c_{p,w}$	groundwater heat capacity ($J \cdot kg^{-1} \cdot °C^{-1}$)
d_h	hydraulic pipe diameter (m)
f_D	Darcy friction factor
g	acceleration of gravity ($m \cdot s^{-2}$)
H_{GT}	position of groundwater table (m)
h	height above groundwater table (m)
h_{eff}	equivalent convective coefficient of pipe wall ($W \cdot m^{-2} \cdot °C^{-1}$)
h_i	convection coefficient inside pipe ($W \cdot m^{-2} \cdot °C^{-1}$)
k_{eff}	effective ground thermal conductivity ($W \cdot m^{-1} \cdot °C^{-1}$)
k_f	fluid thermal conductivity ($W \cdot m^{-1} \cdot °C^{-1}$)
k_p	pipe thermal conductivity ($W \cdot m^{-1} \cdot °C^{-1}$)
Nu	Nusselt number

m	fitting parameter of matrix suction function
n	fitting parameter of matrix suction function
Pr	Prandtl number
Q_{BHE}	thermal load of BHE (W)
$Q_{Building}$	building load (W)
Q_{wall}	heat flux through pipe wall ($W \cdot m^{-2}$)
Re	Reynolds number
r_i	internal radius of pipe (m)
r_o	external radius of pipe (m)
T	ground temperature (℃)
T_{amp}	amplitude of annual temperature (℃)
T_{ext}	temperature outside pipe (℃)
T_f	temperature of circulating fluid (℃)
$T_{f,i}$	inlet fluid temperature (℃)
$T_{f,o}$	outlet fluid temperature (℃)
T_{mean}	annual average temperature (℃)
t	time (s)
t_0	period of one year (s)
u	circulating fluid velocity ($m \cdot s^{-1}$)
u_a	pore air pressure (Pa)
u_w	pore water pressure (Pa)
v_w	groundwater flow velocity ($m \cdot s^{-1}$)

V_f volumetric flow rate ($m^3 \cdot s^{-1}$)

Greek Letters

α_{eff} effective ground thermal diffusivity ($m^2 \cdot s^{-1}$)

η soil porosity

θ volumetric water content

θ_r residual water content

θ_s saturated water content

ρ_f fluid density ($kg \cdot m^{-3}$)

ρ_w groundwater density ($kg \cdot m^{-3}$)

$(\rho c_p)_{eff}$ effective volumetric heat capacity ($J \cdot m^{-3} \cdot °C^{-1}$)

φ phase angle (rad)

X_{air} volume fraction of air

X_{solid} volume fraction of solid

X_{water} volume fraction of water

ψ matric suction (Pa)

Abbreviations

BHE borehole heat exchanger

COP coefficient of performance

GSHP ground source heat pump

Table Captions

Table 1. Parameters of the test site in literature.

Table 2. Parameters used in the numerical study.

Figure Captions

Fig. 1. Diagram of the ground source heat pump system.

Fig. 2. Calculation flow chart of the proposed numerical model.

Fig. 3(a). Comparison of the outlet fluid temperature calculated by proposed numerical model and reported by Hu [47].

Fig. 3(b). Comparison between proposed numerical model and Hu's model [47] when groundwater flow is considered.

Fig. 4. Schematic of the computational soil domain, dimensions in (m).

Fig. 5. Effective soil thermal conductivity and heat capacity with volumetric water content.

Fig. 6. The building load and ground surface temperature.

Fig. 7. Results of the grid independent test.

Fig. 8. Inlet and outlet fluid temperatures with and without heat pump.

Fig. 9. Effect of moisture in unsaturated soil: (a) Outlet fluid temperatures for two BHE lengths, (b) Heat pump COP for two BHE lengths.

Fig. 10. The performance of GSHP system at different groundwater tables: (a) Outlet fluid temperatures, (b) Heat pump COP.

Fig. 11. Four typical groundwater table fluctuation curves.

Fig. 12. Impact of groundwater table fluctuation on the GSHP system: (a) Outlet fluid temperatures, (b) Heat pump COP.

Fig. 13. Effect of groundwater flow rates on the performance of GSHP system considering groundwater tables: (a) Outlet fluid temperatures, (b) Heat pump COP.

Table 1. Parameters of the test site in [47].

Item	Value
Soil thermal conductivity (backfill soil, clay, fine sand), k	2.12, 1.20, 1.61 $W \cdot m^{-1} \cdot ℃^{-1}$
Soil thermal capacity (backfill soil, clay, fine sand), ρc	1.71, 3.74, 2.77 $MJ \cdot m^{-3} \cdot ℃^{-1}$
Initial ground temperature, T	15.5 ℃
Thermal conductivity of pipe wall, k_p	0.45 $W \cdot m^{-1} \cdot ℃^{-1}$
Fluid thermal conductivity, k_f	0.60 $W \cdot m^{-1} \cdot ℃^{-1}$
Fluid thermal capacity, $\rho_f c_{p,f}$	4.20 $MJ \cdot m^{-3} \cdot ℃^{-1}$
Fluid velocity inside BHE, u	0.38 $m \cdot s^{-1}$

Table 2. Parameters used in the numerical study.

Item	Value
Ground components thermal conductivity (air, water, soil particle), k_i	0.026, 0.56, 4 $W \cdot m^{-1} \cdot ℃^{-1}$
Ground components thermal capacity (air, water, soil particle), $\rho_i c_i$	0.00125, 4.2, 2.08 $MJ \cdot m^{-3} \cdot ℃^{-1}$
Thermal conductivity of pipe wall, k_p	0.6 $W \cdot m^{-1} \cdot ℃^{-1}$
Fluid velocity inside BHE, u	0.4 $m \cdot s^{-1}$
Residual water content, θ_r	0.061
Saturated water content, θ_s	0.43

VG model parameter, a	0.012
VG model parameter, *n*	1.39
Annual average temperature, T_{mean}	18.2 ℃
Amplitude of annual temperature, T_{amp}	19.8 ℃
Phase angle, φ	-π/2 rad
COP function coefficients *a'*, *b'*, *c'*	-0.003, 0.056, 5.784 for cooling
	-0.001, 0.133, 3.257 for heating

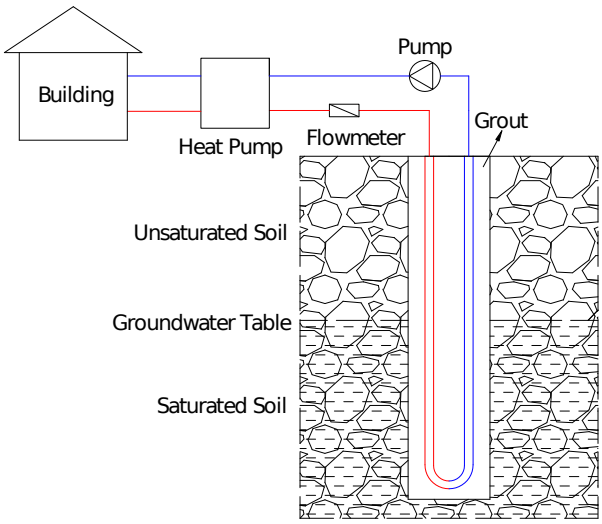

Fig. 1. Diagram of the ground source heat pump system.

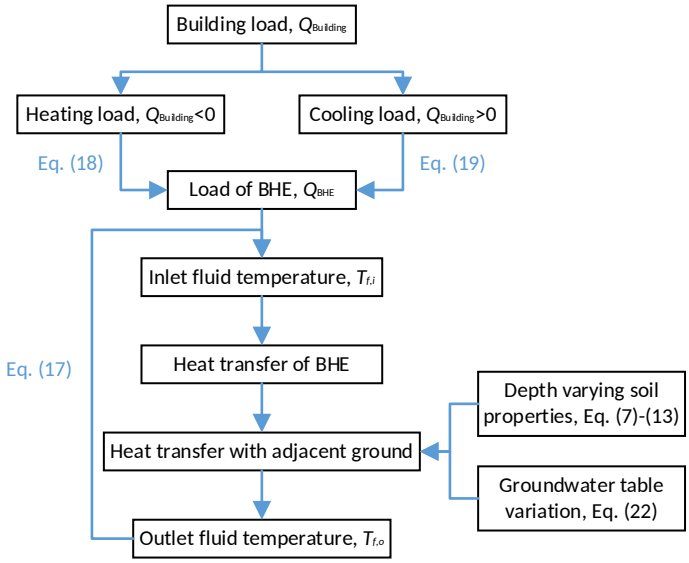

Fig. 2. Calculation flow chart of the proposed numerical model.

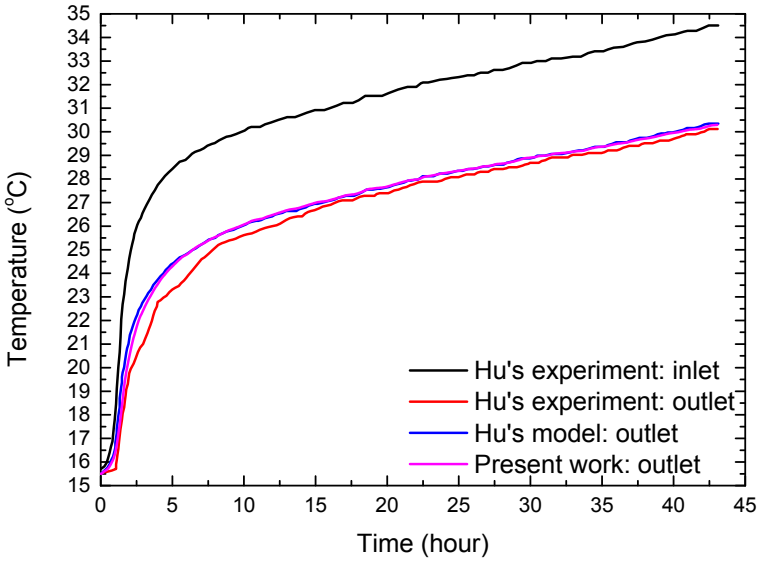

Fig. 3(a). Comparison of the outlet fluid temperature calculated by proposed numerical model and reported by Hu [47].

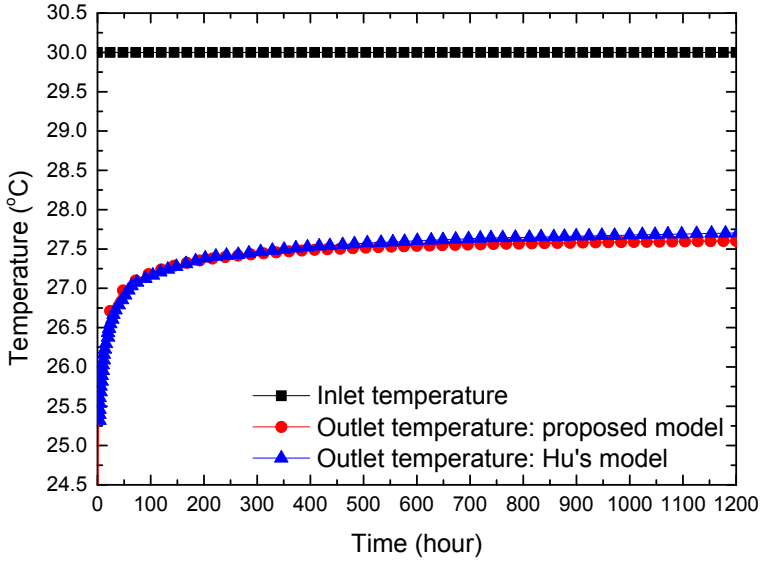

Fig. 3(b). Comparison between proposed numerical model and Hu's model [47] with consideration of groundwater flow.

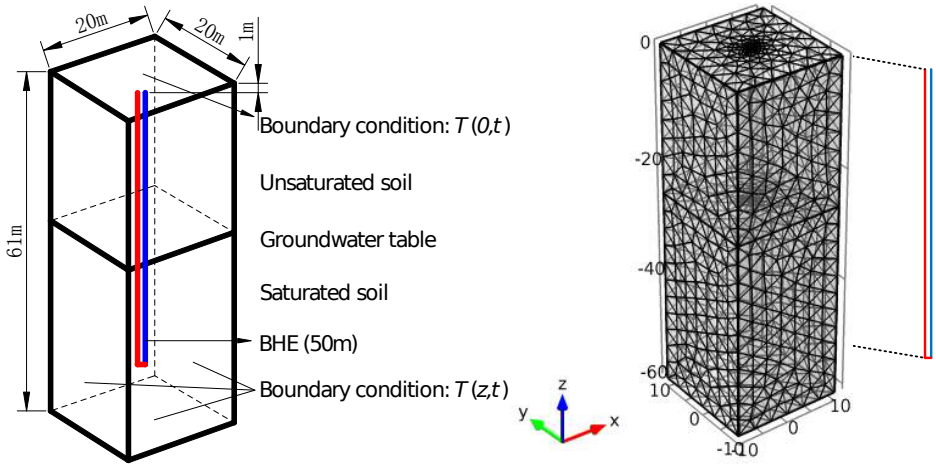

Fig. 4. Schematic of the computational soil domain, dimensions in (m).

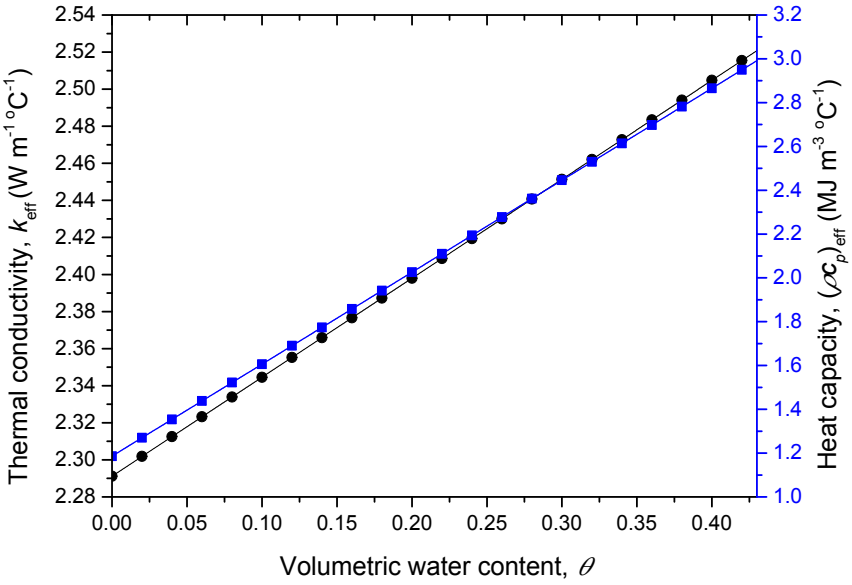

Fig. 5. Effective soil thermal conductivity and heat capacity with volumetric water content.

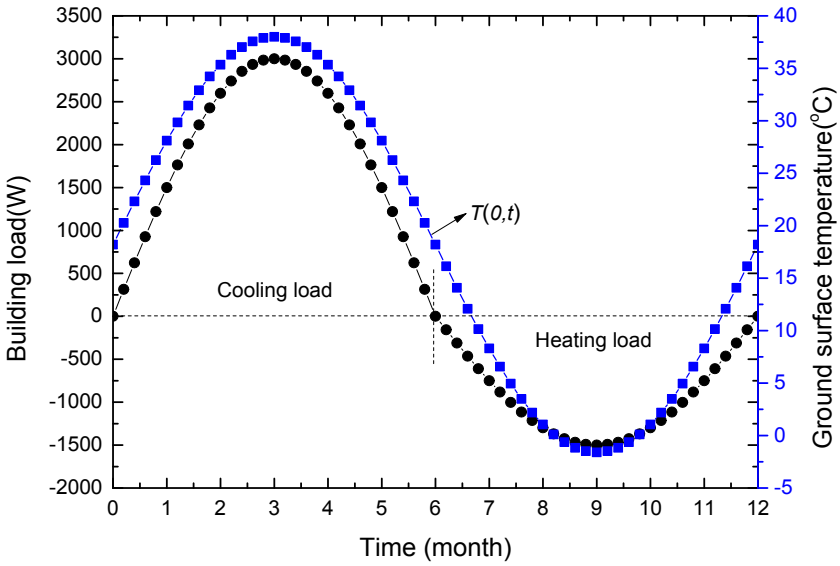

Fig. 6. Building load and ground surface temperature.

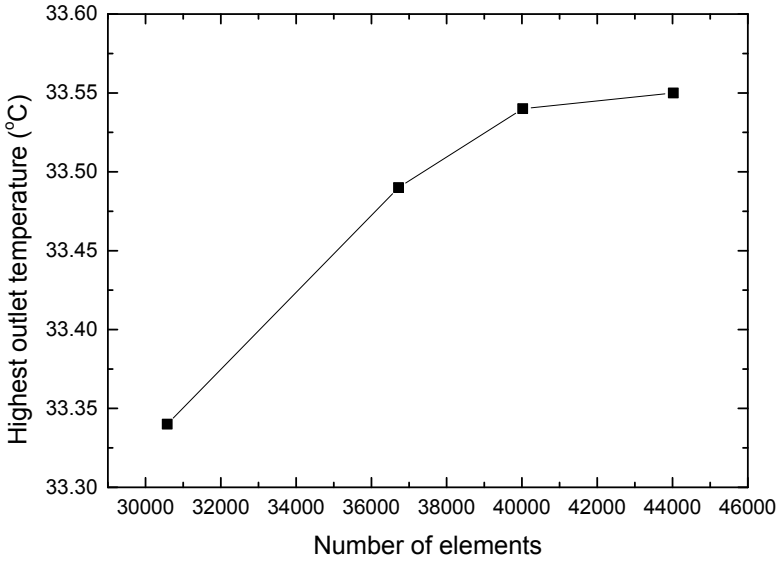

Fig. 7. Results of the grid independent test.

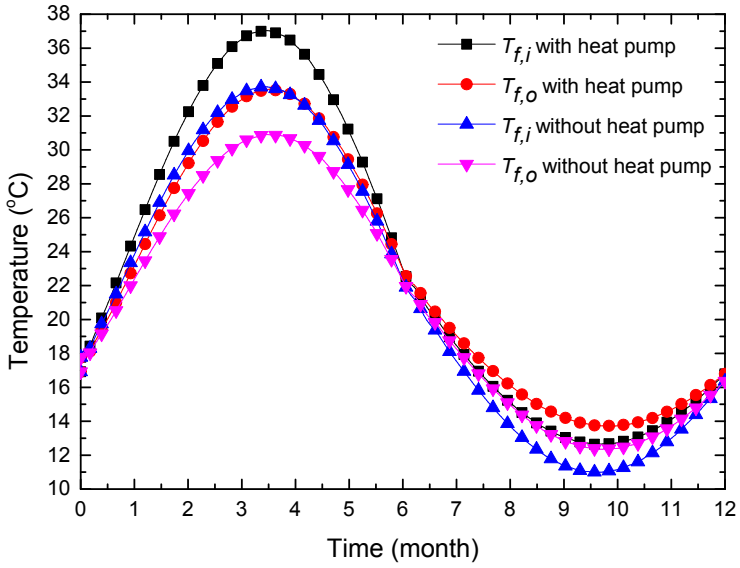

Fig. 8. Inlet and outlet fluid temperatures with and without heat pump.

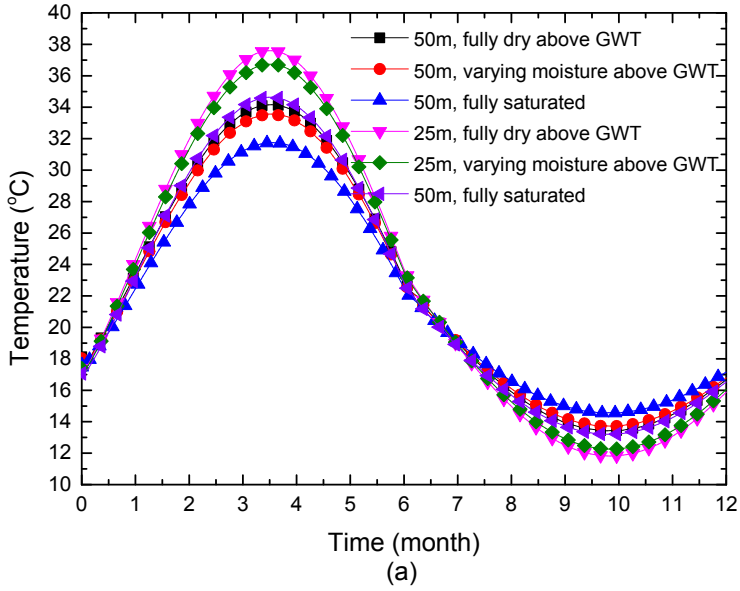

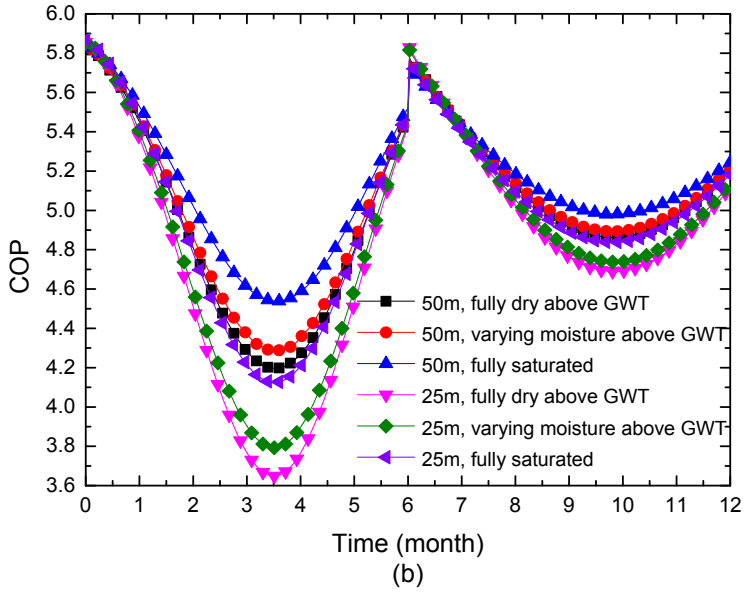

Fig. 9. Effect of moisture in unsaturated soil: (a) Outlet fluid temperatures for two BHE lengths, (b) Heat pump COP for two BHE lengths.

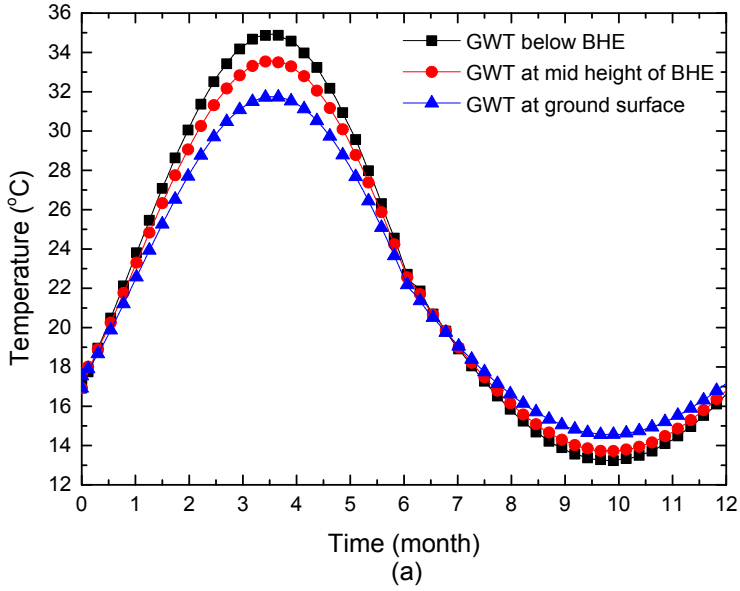

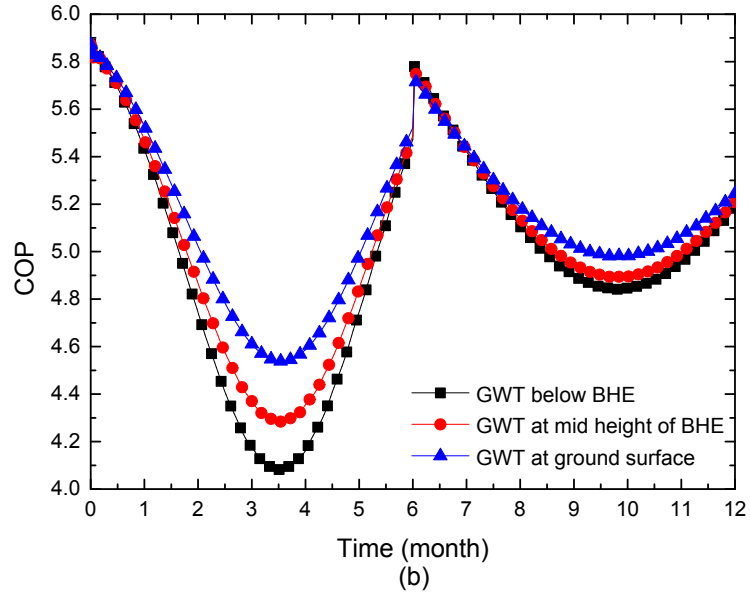

Fig. 10. Performance of GSHP system at different groundwater tables: (a) Outlet fluid temperatures, (b) Heat pump COP.

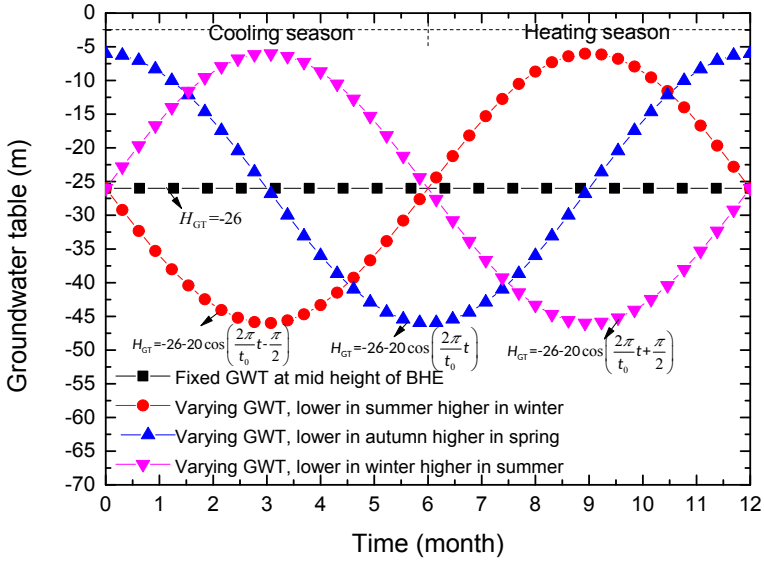

Fig. 11. Four typical groundwater table fluctuation curves.

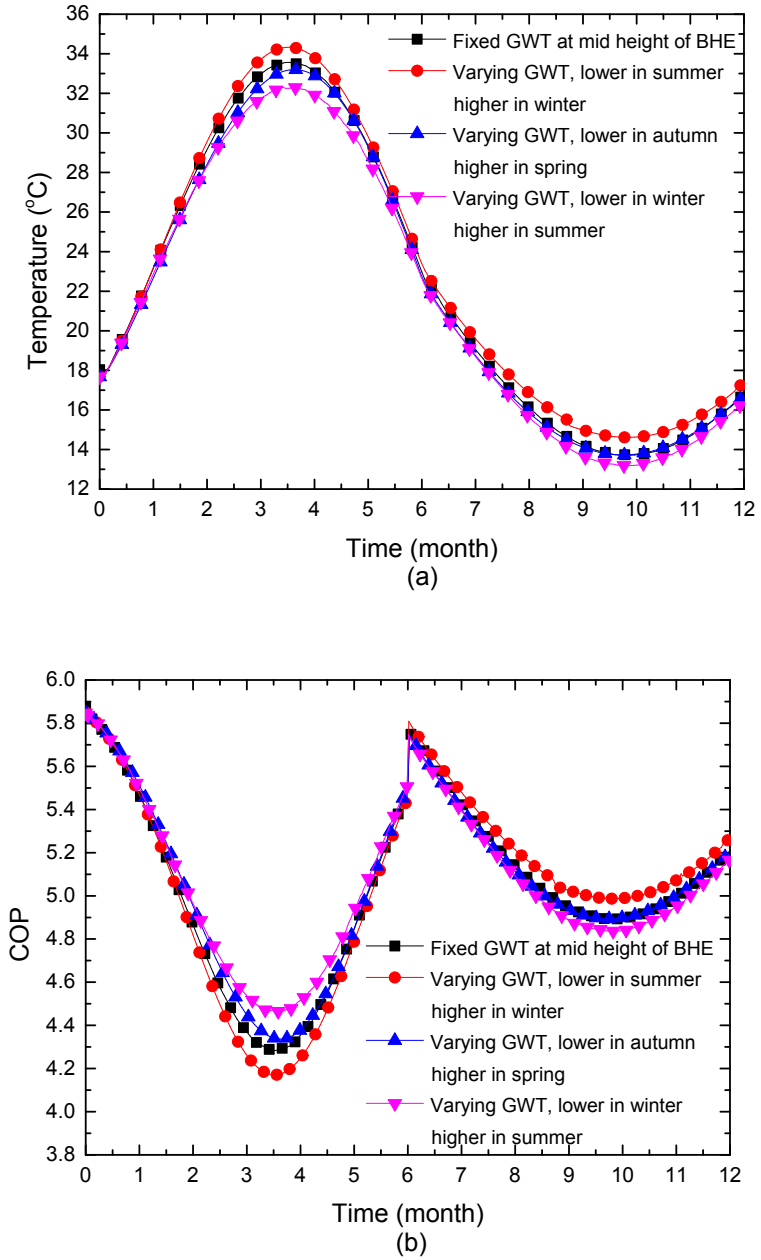

Fig. 12. Impact of groundwater table fluctuation on the GSHP system: (a) Outlet fluid temperatures, (b) Heat pump COP.

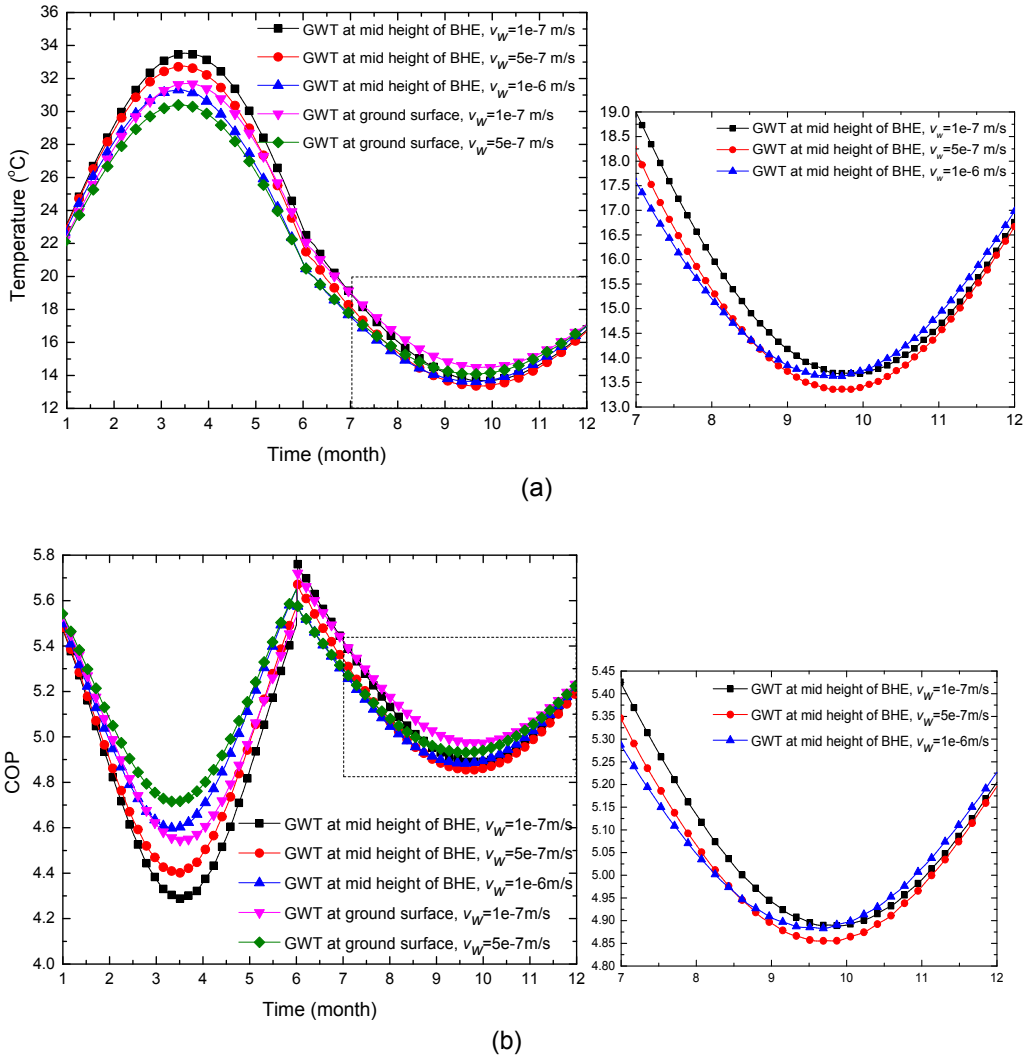

Fig. 13. Effect of groundwater flow rates on the performance of GSHP system considering groundwater tables: (a) Outlet fluid temperatures, (b) Heat pump COP.